Solid-State Molecular Organization and Solution Behavior of Methane-1,1-Diphosphonic Acid Derivatives of Heterocyclic Amines: The Role of the Topochemical Ring Modification and the Intramolecular Hydrogen Bonds in Monosubstituted Piperid-1-ylmethane-1,1-diphosphonic Acids

Ewa Matczak-Jon,*[a] Veneta Videnova-Adrabińska,*[a] Agnieszka Burzyńska,[a] Paweł Kafarski,[a] and Tadeusz Lis[b]

Abstract: The crystal structures of 3-methylpiperid-1-ylmethane-1,1-diphosphonic (**2**), 4-methylpiperid-1-ylmethane-1,1-diphosphonic (**3**), 2-ethylpiperid-1-ylmethane-1,1-diphosphonic (**4**), and 2-methylpiperid-1-ylmethane-1,1-diphosphonic (**5**) acids have been determined and are discussed with respect to their molecular organization and crystal-packing preferences. The chair conformation, predominant also in solution, favors equatorial positioning of the bulky subsituents of the heterocyclic N and C atoms. The molecular geometry also provides access to intramolecular hydrogen-bond formation between the axial protons located on the nitrogen atoms, as well as the carbon atoms closest to it, and phosphonic/phosphonate oxygen atoms. The molecules preferably arrange in monolayers, observed in all crystals with an exception of **3**. The layers are held in place in the third direction through van der Waals interactions. The analysis of two-dimensional hydrogen-bonded networks is concentrated on revealing how the substituent's topology of the molecule affects the solid-state organization in well-defined structures and is aimed at unraveling the consequences and the possible conformational changes by stepwise network disruption upon crystal dissolution in water. The solution NMR studies are focused on revealing the role that the topochemistry of the substituent plays for the stereodynamics in **2**–**5**. It is demonstrated that in constrast to piperid-1-ylmethane-1,1-diphosphonic acid (**1**), in which the ring inversion/rotation around the C–N bond concerted with the N–H···O hydrogen-bond breaking/formation process leads to a mixture of two interconverting conformers, the concerted N–H···O breaking/rotation/N–H···O formation process in **2** and **3** allows for a predominance of one conformer in solution. However, placement of a substituent at 2-position in the ring hampers the rotation around the C–N bond; this makes **4** and **5** significantly less flexible relative to compounds **1**–**3**. In addition, both compounds **4** and **5** are proved to exist as a mixture of two conformers, the equilibrium of which in acidic solution is shifted towards the conformer found in solid state. In alkaline solutions of **4** and **5**, the equilibrium is shifted towards the conformer that is forced by the flipping of the heterocyclic ring. These results correlate well with recently documented differences in the biological potency of this group of compounds.

Keywords: bisphosphonates · conformation analysis · hydrogen-bonds · NMR spectroscopy · self-assembly · X-ray diffraction

Introduction

Bisphosphonates constitute an interesting class of hydrolytically stable analogues of pyrophosphate, in which the oxygen bridge between the phosphorus atoms is replaced by a carbon atom, with the possibility to attach specific side chains to it. For over two decades they have been employed as therapeutic agents for treatment of bone disorders characterized by an excessive bone turnover, such as Paget's disease, hypercalcemia of malignancy, and osteoporosis.[1] De-

[a] Dr. E. Matczak-Jon, V. Videnova-Adrabińska, Dr. A. Burzyńska, Prof. P. Kafarski
Department of Chemistry, Wrocław University of Technology
Wybrzeże Wyspiańskiego 27, 50–370 Wrocław (Poland)
Fax: (+48) 71-328-4330
E-mail: jon@ichn.ch.pwr.wroc.pl
veneta@ichn.ch.pwr.wroc.pl

[b] Prof. T. Lis
Faculty of Chemistry, University of Wrocław
Joliot-Curie 14, 50–383 Wrocław (Poland)

 DOI: 10.1002/chem.200400348

spite the large amount experimental data referring their activity, the molecular mode of their action still remains unclear. An important breakthrough in understanding the molecular mechanism by which bisphosphonates inhibit bone resorption was the discovery that drugs possessing a nitrogen atom in their side chain may inhibit the intracellular mevalonate pathway. In particular, the farnesyl pyrophosphate synthase (FPPS) was identified as their principal target.[2] The reduction in the farnesyl pyrophosphate level inhibits the prenylation of the intracellular signaling proteins and thereby impairs many cellular functions, which in turn leads to a programmed cell death.[2a,3]

Along with their well-documented treating properties for bone disorders, bisphosphonates have also been identified as potent antiparasitic agents.[4] They were shown to combat parasitic protozoa, which are the causative agents of human African trypanosomiasis (sleeping sickness), malaria, and visceral leishmaniasis. The initial studies on nitrogen-containing bisphosphonates were limited to compounds directly used in bone resorption therapy.[4a] Structurally diverse compounds, including the aminomethane-1,1-diphosphonic acids (alternatively named aminomethylenebisphosphonic acids) with nitrogen directly bonded to C_α[4b–e] are of current interest. The antiparasitic activity of all these compounds can also be attributed to the inhibition of the farnesyl pyrophosphate synthase.[5]

Finally, the group of substituted aminomethane-1,1-diphosphonic acids constitute a new class of promising herbicides with remarkable phytotoxic effects at both the whole plant and cell culture level.[6] However, the attempts to define mechanism of their action give quite contradictory results, indicating that the mode of their herbicidal activity is complex and presumably relies on the simultaneous action on several plant enzymes, including the farnesyl pyrophosphate synthase.[7]

The studies on the structure–activity relationship[4c–e,5a,8] show that the key feature for the FPPS inhibition is the presence of the nitrogen atom. Its positive charge appears to be very important, since it mimics reactive carbocation intermediates of the enzyme-catalyzed reaction. The spatial accessibility of the positively charged nitrogen atom may also play role. On the other hand, the nature and the size of the substituent on N are crucial for the compound activity as well. Sufficiently bulky substituents introduce a good steric contact with the active site of the enzyme. Generally, aromatic substituents, providing the system with hydrophobicity and charge delocalisation, are considered to be more effective than non-aromatic ones. Despite the significant progress made in understanding the inhibitory properties of bisphosphonates, it is still less studied and it is not well understood why relatively small modifications in their structure may lead to significant changes in their biological potency.

Previously, we demonstrated that the combination of X-ray diffraction analysis and solution NMR studies gives a powerful tool for revealing the inherent molecular properties of bisphosphonates.[9] The disentanglement of the crystal networks based on the priorities of the hydrogen-bond formations and the hierarchy in the molecular organization allowed us to deduct the preferred association forms of these compounds in solution. Although the used methodology may be argued, considering the not exactly understood solution/solid-state relationship, it appears to be very helpful for uncovering the grounds of the chemical functionality and, possibly, the biological activity. Such a strategy can be considered as an inverse to the crystal engineering strategy.

Our present studies concern piperid-1-ylmethane-1,1-diphosphonic acid (**1**)[10] and a group of its derivatives (**2**–**5**) with a topologically modified piperidine ring. In particular, we are aim to reveal the structure-dependent relationships of the inter- and intramolecular hydrogen bonds, which appear to play an essential role for the solution behavior of these compounds.

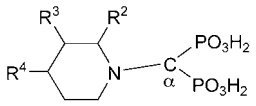

1 $R^2 = R^3 = R^4 = H$
2 $R^3 = Me$, $R^2 = R^4 = H$
3 $R^4 = Me$, $R^2 = R^3 = H$
4 $R^2 = Et$, $R^3 = H$, $R^4 = H$
5 $R^2 = Me$, $R^3 = H$, $R^4 = H$

Very recently the compounds **1**–**5** have been shown to act as immunomodulators that activate the γδT cell, playing an important role in the immune system. Although the mechanism of this activation is not clear yet, it appears again to be highly correlated with the activity of bisphosphonates as FPPS inhibitors.[11] The order of the decreasing activities for **1**–**5** expressed in IC_{50} values (IC_{50}: concentration (μM) for 50% stimulation) has been shown to be the following: **3** > **1** > **2** ⩾ **4** ⩾ **5**. The IC_{50} values are in the range from 24 for **3** to 1203 and 2741 for **4** and **5**, respectively.

In view of this, it seems reasonable to look for the molecular basis of the above reported results with respect to the topochemical relations and the aggregational predisposition of the compounds. Therefore, the present studies are targeted at discerning the stereodynamics in **1**–**5**, taking their conformational similarities and dissimilarities into consideration.

Results and Discussion

Solid-state molecular organization: The molecular structures, atomic numbering scheme and the intramolecular hydrogen-bond connectivity patterns for **2**–**5** are shown in Figure 1. For comparison purposes the atom numbering of the phosphonic and the phosphonate groups is consistent with that of the formerly studied *N*-substituted aminomethane-1,1-diphosphonic acids.[9] Compounds **2**, **3**, and **5**,

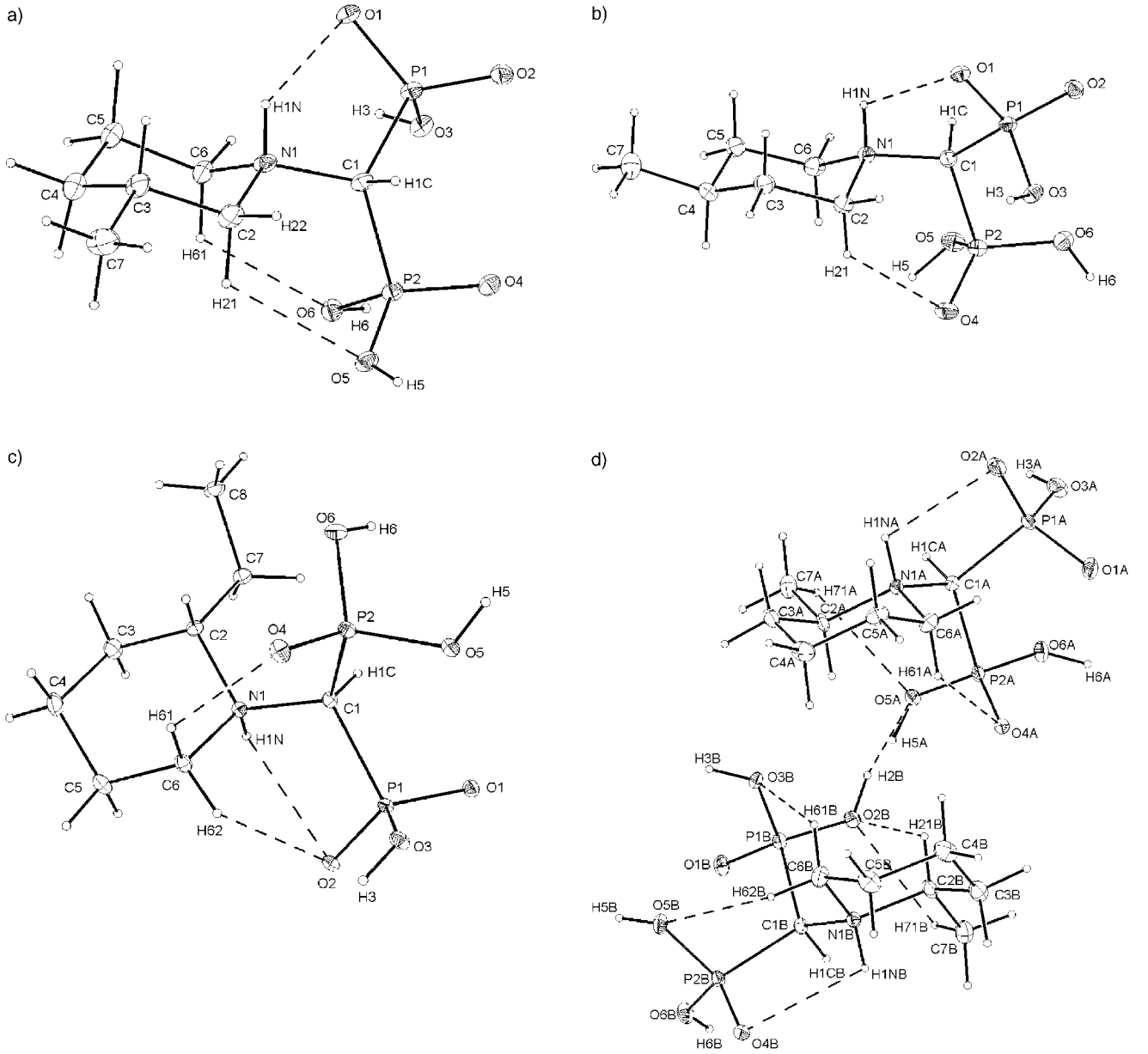

Figure 1. Molecular structure and crystallographic numbering scheme of compounds **2**–**5**: a) 3-methyl-piperid-1-ylmethane-1,1-diphosphonic acid; b) 4-methyl-piperid-1-ylmethane-1,1-diphosphonic acid; c) 2-ethyl-piperid-1-ylmethane-1,1-diphosphonic acid; d) 2-methyl-piperid-1-ylmethane-1,1-diphosphonic acid. The displacement ellipsoids are at 40% probability level. Water molecules are omitted for clarity.

are crystallographically isostructural with the unsubstituted piperid-1-ylmethane-1,1-diphosphonic acid[10] (**1**) and crystallize in the monoclinic $P2_1/n$ space group. Compound **4** crystallizes in the triclinic space group $P\bar{1}$ (Table 1). Similar to the *N*-substituted aminomethane-1,1-diphosphonic acids,[9] all the studied compounds appear in a zwitterionic form with a proton transferred from one of the phosphonic groups towards the nitrogen atom (N1). The heterocyclic ring in all compounds adopts a chair conformation with an equatorial alkyl substituent on the ring C atom and an axial hydrogen atom (H1N) on the nitrogen atom. The multiple intramolecular hydrogen bonds, established between the axial ring hydrogen atoms (located on N and the closest C atoms) and one or both phosphonic/phosphonate groups, generate rigid hydrogen-bonded motifs S(5) and S(6).

The most important structural parameters are presented in Table 2. A careful analysis of these data reveals very close similarities of the internal molecular parameters of **2** and **3** relative to those of **1**. For the reasons of space we will not discuss the intramolecular relations of these compounds in detail and refer the readers to Table 2 and the supplementary crystallographic data (see Experimental Section). The main focus of the discussion considers the organizational features of the studied compounds in solid state with respect to the most abundant molecular associations in solution and their impact on the solution properties.

Table 1. Summary of crystal data, data collection, and refinement conditions for compounds **2**–**5**.

	2	**3**	**4**	**5**
formula	$C_7H_{17}NO_6P_2$	$C_7H_{23}NO_9P_2$	$C_8H_{21}NO_7P_2$	$C_7H_{19.5}NO_{7.25}P_2$
M_r	273.16	327.2	305.20	295.68
crystal system	monoclinic	monoclinic	triclinic	monoclinic
space group	$P2_1/n$	$P2_1/n$	$P\bar{1}$	$P2_1/n$
a [Å]	6.444(2)	5.974(2)	7.001(3)	8.988(2)
b [Å]	8.119(3)	14.398(4)	7.864(3)	14.703(3)
c [Å]	20.401(5)	17.548(4)	12.035(4)	18.688(4)
α [°]			72.71(3)	
β [°]	92.69(3)	92.11(3)	89.48(3)	96.44(3)
γ [°]			83.73(3)	
V [Å^3]	1066.2(6)	1508.3(7)	628.7(4)	2454.0(9)
T [K]	100(2)	100(2)	100(2)	100(2)
Z	4	4	2	8
ρ_{calcd} [g cm^{-3}]	1.702	1.441	1.612	1.601
$\mu(Mo_{K\alpha})$ [mm^{-1}]	0.422	0.325	0.373	0.381
θ range [°]	3.91–35.69	3.65–35.18	3.55–35.60	3.29–35.27
reflections collected	15752	19210	12103	29308
independent reflections (R_{int})	4581 (0.0894)	5996 (0.0819)	4939 (0.0319)	8824 (0.0836)
reflections observed [$I>2\sigma(I)$]	2706	3480	3869	5140
refined parameters	212	264	247	395
R[a]	0.0693	0.0752	0.0378	0.0764
$wR2$[b]	0.0948	0.0825	0.0879	0.0779
all data R	0.1552	0.1638	0.0569	0.1660
$wR2$	0.1164	0.0998	0.0951	0.0950
$\Delta\rho_{min}/\Delta\rho_{max}$ [e Å^{-3}]	−0.51/0.52	−0.41/0.36	−0.48/0.55	−0.42/0.38

[a] $R=\Sigma(F_o-F_c)/\Sigma F_o$. [b] $wR2=[\Sigma w(F_o^2-F_c^2)^2/\Sigma w(F_o^2)^2]^{1/2}$.

arranged in (001) molecular monolayers with hydrophilic interior and hydrophobic exterior. The solid-state molecular conformation is firmly fixed by three rigid ring motifs (S(5) and S(6)) formed by the intramolecular hydrogen bonds N1−H1N···O1, C6-H61···O6, and C2−H21···O5 (assigned as 9, 10, and 11) (see Figure 1a and Table 3). This configuration sets a predisposition for a mutual recognition of the identical sites (phosphonic–phosphonic or phosphonate–phosphonate).

The molecular dimer formed by O3−H3···O1 (assigned as 1) with an eight-membered ring motif R2,2(8) can be considered as the smallest building block of the crystal. Two different N–phosphonate hydrogen-bond interactions (2 and 3) are used to extend the inversion-related dimeric units into molecular ribbons along the *a* direction (Figure 2a). An additional four-membered ring is generated along the ribbon from the combination of the inter- and intramolecular N–phosphonate hydrogen bonds (3 and 9). The two phosphonic groups are alternately arranged on both sides of the ribbons and provide

The crystal network of ***2***: The substitution of one of the ring C3 hydrogen atoms for the methyl group does not change the molecular organization in the crystal significantly. The three-dimensional hydrogen-bonded network of **2** is identical with that of **1**[10] (see Tables 2 and 3). The molecules are

Table 2. Selected intramolecular bond lengths [Å], angles [°] and torsion angles [°] for compounds **1**–**5**.

	1[10][a]	**2**	**3**	**4**	**5**	
					A-unit	B-unit
P1−O1	1.511(3)	1.505(2)	1.515(2)	1.5076(12)	1.522(2)	1.511(2)
P1−O2	1.506(3)	1.501(2)	1.495(2)	1.5010(12)	1.484(2)	1.532(2)
P1−O3	1.572(3)	1.569(2)	1.571(2)	1.5757(12)	1.561(2)	1.522(2)
P1−C1	1.854(4)	1.853(3)	1.845(2)	1.866(2)	1.852(3)	1.846(3)
P2−O4	1.496(3)	1.488(2)	1.481(2)	1.4809(12)	1.501(2)	1.484(2)
P2−O5	1.549(3)	1.543(2)	1.531(2)	1.5496(12)	1.511(2)	1.539(2)
P2−O6	1.544(3)	1.548(2)	1.546(2)	1.5628(12)	1.568(2)	1.546(2)
P2−C1	1.830(3)	1.838(3)	1.852(2)	1.842(2)	1.846(3)	1.853(2)
N1−C1	1.514(5)	1.520(3)	1.519(3)	1.523(2)	1.530(3)	1.526(3)
N1−C2	1.509(5)	1.504(3)	1.514(3)	1.537(2)	1.533(3)	1.538(3)
N1−C6	1.505(5)	1.507(3)	1.514(3)	1.518(2)	1.517(3)	1.524(4)
P1-C1-P2	111.6(2)	111.73(12)	115.42(11)	114.31(7)	116.71(15)	113.89(12)
N1-C1-P1	111.6(2)	110.9(2)	111.49(14)	111.10(9)	108.3(2)	117.5(2)
N1-C1-P2	118.9(3)	118.6(2)	114.54(14)	114.98(8)	115.3(2)	109.41(15)
C1-N1-C2	111.7(3)	112.7(2)	115.0(2)	114.95(10)	114.3(2)	114.4(2)
C1-N1-C6	115.3(3)	115.2(2)	113.7(2)	112.10(10)	111.8(2)	111.8(2)
C2-N1-C6	110.8(3)	110.1(2)	109.7(2)	108.63(10)	110.6(2)	110.6(2)
O2-P1-C1-N1	136.3(2)	137.7(2)	−147.6(2)	14.82(10)	−29.0(2)	66.9(2)
O4-P2-C1-N1	176.8(3)	175.5(2)	−45.9(2)	45.94(11)	−51.7(2)	−30.9(2)
C2-N1-C1-P1	−155.3(2)	−160.2(2)	−64.3(2)	−171.77(9)	168.0(2)	−58.0(3)
C2-N1-C1-P2	72.5(4)	68.5(2)	69.1(2)	56.42(13)	−59.0(2)	170.1(2)
C6-N1-C1-P1	77.1(3)	72.3(2)	168.1(2)	63.53(12)	−65.4(2)	68.8(2)
C6-N1-C1-P2	−55.1(4)	−58.9(2)	−58.5(2)	−68.28(12)	67.5(2)	−63.1(2)

[a] The original crystal numbering scheme has been changed in order to make it consistent with that of the studied compounds.

Table 3. Hydrogen-bond geometries and hydrogen-bond patterns of compounds **1**–**5**.

	H-bond interactions		H···A [Å]	D···A [Å]	∢DHA [°]	Symmetry code	H-Bond motif
	piperid-1-ylmethane-1,1-diphosphonic acid (**1**)[10][a]						
	acid–acid H-bonds						
	molecular ribbons along the *a* direction					inversion and translation	
1	O3−H3···O1	phosphonate–phosphonate	1.78	2.599(4)	163	2−*x*, 2−*y*, −*z*	R2,2(8)
2	N1−H1N···O2	N–phosphonate	2.30	3.056(4)	151	2−*x*, 1−*y*, −*z*	R2,2(10)
	molecular monolayers (001)					translation along the *b* axis	
3	O6−H6···O4	phosphonic–phosphonic	1.67	2.502(4)	169	1−*x*, 2−*y*, −*z*	R2,2(8)
4	O5−H5···O2	phosphonic–phosphonate	1.73	2.536(4)	159	1−*x*, 1−*y*, −*z*	R2,2(12)
	stabilizing interactions						
5	C1−H1C···O4	C_α–phosphonic	2.22	3.076(4)	143	1−*x*, 1−*y*, −*z*	
6	C1−H1C···O1	C_α–phosphonate	2.42	3.045(5)	120	2−*x*, 1−*y*, −*z*	
7	C3−H31···O2	C_{ring}–phosphonate	2.51	3.301(5)	137	2−*x*, 1−*y*, −*z*	
	intramolecular H-bonds		conformational stabilization				
8	N1−H1N···O1	N–phosphonate	2.35	2.867(5)	121	*x*, *y*, *z*	S(5)
9	C6−H61···O1	C_{ring}–phosphonic	2.40	2.988(4)	118	*x*, *y*, *z*	S(6)
10	C2−H21···O5	C_{ring}–phosphonic	2.54	3.213(4)	125	*x*, *y*, *z*	S(6)
	3-methyl-piperid-1-ylmethane-1,1-diphosphonic acid (**2**)						
	acid–acid H-bonds						
	molecular ribbons along the *a* direction					inversion and translation	
1	O3−H3···O1	phosphonate–phosphonate	1.80(4)	2.623(2)	179(5)	1−*x*, 1−*y*, 1−*z*	R2,2(8)
2	N1−H1N···O2	N–phosphonate	2.23(3)	3.111(3)	158(2)	2−*x*, 1−*y*, 1−*z*	R2,2(10)
3	N1−H1N···O1	N–phosphonate	2.51(3)	3.113(3)	123(2)	2−*x*, 1−*y*, 1−*z*	R2,2(10)
	molecular monolayers (001)					translation along the *b* axis	
4	O6−H6···O4	phosphonic–phosphonic	1.69(4)	2.519(2)	163(4)	1−*x*, −*y*, 1−*z*	R2,2(8)
5	O5−H5···O2	phosphonic–phosphonate	1.90(4)	2.552(2)	172(4)	2−*x*, −*y*, 1−*z*	R2,2(12)
	stabilizing interactions						
6	C1−H1C···O4	C_α–phosphonic	2.24(3)	3.084(3)	150(2)	2−*x*, −*y*, 1−*z*	
7	C3−H31···O2	C_{ring}–phosphonate	2.47(2)	3.332(3)	140(2)	2−*x*, 1−*y*, 1−*z*	
8	C1−H1C···O1	C_α–phosphonate	2.53(3)	3.040(3)	115(2)	2−*x*, 1−*y*, 1−*z*	
	intramolecular H-bonds		conformational stabilization				
9	N1−H1N···O1	N–phosphonate	2.39(3)	2.862(3)	111(2)	*x*, *y*, *z*	S(5)
10	C6−H61···O6	C_{ring}–phosphonic	2.40(2)	3.023(3)	119(2)	*x*, *y*, *z*	S(6)
11	C2−H21···O5	C_{ring}–phosphonic	2.56(3)	3.184(3)	118(2)	*x*, *y*, *z*	S(6)
	4-methyl-piperid-1-ylmethane-1,1-diphosphonic acid (**3**)						
	acid–acid H-bonds						
	molecular dimers					inversion	
1	O3−H3···O1	phosphonate–phosphonate	1.67(3)	2.570(2)	176(3)	−*x*, 1−*y*, 1−*z*	R2,2(8)
	molecular ribbons along the *a* direction					translation along the *a* axis	
2	N1−H1N···O1	N–phosphonate	1.91(3)	2.790(2)	154(3)	1−*x*, 1−*y*, −*z*	R2,2(10)
	water H-bonds, 3D network						
3	O5−H5···O3w	phosphonic–water	1.37(4)	2.416(2)	171(4)	*x*, *y*, *z*	
4	O6−H6···O1w	phosphonic–water	1.60(3)	2.529(3)	174(3)	−0.5−*x*, −0.5+*y*, 0.5−*z*	
5	O3w−H6w···O2w	water–water	1.73(4)	2.632(3)	173(3)	1+*x*, *y*, *z*	
6	O2w−H3w···O4	water–phosphonic	1.78(3)	2.638(2)	172(3)	*x*, *y*, *z*	
7	O3w−H5w···O2	water–phosphonic	1.78(4)	2.603(3)	170(4)	0.5−*x*, 0.5+*y*, 0.5−*z*	
8	O2w−H4w···O2	water–phosphonate	1.84(4)	2.719(2)	175(3)	0.5−*x*, 0.5+*y*, 0.5−*z*	
9	O1w−H2w···O5	water–phosphonic	1.95(4)	2.801(3)	178(3)	0.5−*x*, 0.5+*y*, 0.5−*z*	
10	O1w−H1w···O2w	water–water	1.99(3)	2.771(3)	166(3)	*x*, *y*, *z*	
	intramolecular H-bonds		conformational stabilization				
11	N1−H1N···O1	N–phosphonate	2.40(3)	2.900(2)	113(2)	*x*, *y*, *z*	S(5)
12	C2−H21···O4	C_{ring}–phosphonic	2.40(2)	3.067(3)	128(2)	*x*, *y*, *z*	S(6)
	2-ethyl-piperid-1-ylmethane-1,1-diphosphonic acid (**4**)						
	acid–acid interactions						
	molecular dimers					inversion	
1	O3−H3···O2	phosphonate–phosphonate	1.76(2)	2.579(2)	177(3)	2−*x*, 1−*y*, 1−*z*	R2,2(8)
	molecular ribbons along the *a* direction					translation along the *a* axis	
2	N1−H1N···O1	N–phosphonate	2.09(2)	2.924(2)	160.4(19)	1−*x*, 1−*y*, 1−*z*	R2,2(10)
	molecular layers (001)					translation along the *b* axis	
3	O5−H5···O1	phosphonic–phosphonate	1.69(3)	2.519(2)	169(3)	1−*x*, 2−*y*, 1−*z*	R2,2(12)
	acid–water interactions		layer stabilization				
4	O6−H6···O1w	phosphonic–water	1.70(3)	2.532(2)	176(2)	*x*, *y*, *z*	
5	O1w−H1w···O4	water–phosphonic	1.93(3)	2.726(2)	178(2)	−1+*x*, *y*, *z*	C(6)
6	O1w−H2w···O3	water–phosphonate	2.16(3)	2.950(2)	163(3)	1−*x*, 2−*y*, 1−*z*	

Table 3. (Continued)

	H-bond interactions		H···A [Å]	D···A [Å]	∢DHA [°]	Symmetry code	H-Bond motif
7	C1–H1C···O2	C_α–phosphonate	2.41(2)	3.222(2)	144(2)	$1-x, 1-y, 1-z$	
8	C7–H71···O1w	C_{ring}–water	2.530(2)	3.417(2)	150(2)	x, y, z	
	intramolecular H-bonds		conformational stabilization				
9	N1–H1N···O2	N–phosphonate	2.509(19)	2.888(2)	107(2)	x, y, z	S(5)
10	C6–H61···O4	C_{ring}–phosphonic	2.356(16)	3.063(2)	128(2)	x, y, z	S(6)
11	C6-H62···O2	C_{ring}–phosphonate	2.434(17)	3.074(2)	125(1)	x, y, z	S(6)
	2-methyl-piperid-1-ylmethane-1,1-diphosphonic acid (**5**)						
	acid–acid interactions						
	asymmetric unit A–B					pseudo screw rotation $2_1(y)$	
1a	O2B–H2B···O5A	phosphonate–phosphonic	1.64(3)	2.479(3)	168(4)	x, y, z	D
1b	O5A–H5A···O2B	phosphonic–phosphonate	1.63(6)	2.479(3)	176(8)	x, y, z	D
	molecular ribbons					translation along the *a* axis	
2	O3B–H3B···O1A	phosphonate–phosphonate	1.55(3)	2.423(2)	171(3)	$1+x, y, z$	C(10)[b]
3	O5B–H5B···O4A	phosphonic–phosphonic	1.60(3)	2.467(2)	176(3)	$1+x, y, z$	C(10)[b]
4	O6A–H6A···O1B	phosphonic–phosphonate	1.75(3)	2.636(2)	170(3)	$-1+x, y, z$	C(8)[b]
	molecular layers (010)					*n*-glide reflection	
5	N1B–H1NB···O2A	N–phosphonate	1.78(3)	2.719(3)	168(3)	$0.5+x, 0.5-y, -0.5+z$	C(11)
6	N1A–H1NA···O4B	N–phosphonic	1.94(3)	2.861(3)	165(2)	$-0.5+x, 0.5-y, 0.5+z$	C(11)
	3D crystal network					inversion	
7	O6B–H6B···O1B	phosphonic–phosphonate	1.76(3)	2.581(3)	174(2)	$2-x, -y, -z$	R2,2(8)
	water H-bond interactions stabilizing the 3D network						
8a	O3A–H3A···O3wB	phosphonate–water	1.66(3)	2.376(10)	171(4)	$0.5-x, -0.5+y, 0.5-z$	
8b	O3A–H3A···O3wA	phosphonate–water	2.16(3)	2.877(9)	172(3)	$0.5-x, -0.5+y, 0.5-z$	
9	O3wA–H5w···O1w	water–water	1.88(3)	2.665(9)	151(3)	$0.5-x, 0.5+y, 0.5-z$	
10	O3wB–H7w···O2w	water–water	1.92(3)	2.743(9)	160(6)	x, y, z	
11	O2w–H4w···O4B	water–phosphonic	1.93(3)	2.782(5)	171(5)	$-1+x, y, z$	
12	O1w–H1w···O1A	water–phosphonate	1.96(3)	2.830(3)	169(3)	$0.5-x, -0.5+y, 0.5-z$	
13	O1w–H2w···O5A	water–phosphonic	2.23(3)	2.970(3)	160(3)	x, y, z	
14	O3wA–H6w···O5B	water–phosphonic	2.30(3)	3.055(9)	147(5)	$-1+x, y, z$	
	intramolecular interactions stabilizing the conformation of the asymmetric A unit						
15	N1A–H1NA···O2A	N–phosphonate	2.39(3)	2.846(3)	109(2)	x, y, z	S(5)
16	C6A–H61···O4A	C_{ring}–phosphonic	2.37	3.069(3)	127	x, y, z	S(6)
17	C7A–H71A···O5A	C_{Me}–phosphonic	2.60(3)	3.226(4)	121(2)	x, y, z	S(7)
	intramolecular interactions stabilizing the conformation of the asymmetric B unit						
18	N1B–H1(NB)···O4B	N–phosphonic	2.52(3)	2.908(3)	105(2)	x, y, z	S(5)
19	C2B–H21B···O2B	C_{ring}–phosphonate	2.54	3.094(3)	115	x, y, z	S(6)
20	C6B–H62B···O5B	C_{ring}–phosphonic	2.56	3.293(3)	131	x, y, z	S(6
21	C6B–H61B···O3B	C_{ring}–phosphonate	2.45	3.131(3)	126	x, y, z	S(6)
22	C7B–H71B···O2B	C_{Me}–phosphonate	2.48(3)	3.171(4)	125	x, y, z	S(7)
	intramolecular interactions stabilizing the conformation of the asymmetric dimer unit A–B						
23	C2A–H21A···O3B	C_{ring}–phosphonate	2.38	3.171(3)	135	x, y, z	D
24	C2B–H21B···O4A	C_{ring}–phosphonic	2.47	3.286(3)	138	x, y, z	D
	intermolecular stabilizing interactions						
25	C5A–H52A···O3A	C_{ring}–phosphonate	2.49	3.482(3)	176	$0.5-x, 0.5+y, 0.5-z$	
26	C5A–H51A···O1B	C_{ring}–phosphonate	2.57	3.299(3)	130	$1.5-x, 0.5+y, 0.5-z$	
27	C1A–H1CA···O3wB	C_α–water	2.56	3.332(10)	134	$0.5-x, -0.5+y, 0.5-z$	

[a] The original crystal numbering scheme has been changed in order to make it consistent with that of the studied compounds. [b] **2** and **3** generate R2,2(12); **3** and **4** generate R2,2(10).

additional recognition sites accessible for inter-ribbon hydrogen-bond interactions with a resultant (001) monolayer formation. Two hydrogen bonds O6–H6···O4 (4) and O5–H5···O2 (5) connect the ribbons in the layer generating new motifs R2,2(8) and R2,2(12) (see Table 3). Due to the inflexibility of the methane-1,1-diphosphonic portion, the inter-ribbon R2,2(8) motif is strongly distorted (Figure 2a). The geometry of bonds 4 and 5 significantly deviates from linearity in order to accommodate the two-dimensional network. The heterocyclic rings in **2**, alternately arranged on both sides of the (001) molecular layers, protrude in a manner so as to fit in the large meshes formed between the ribbons (Figure 2b). The specific molecular conformation of **2** enables a formation of three additional, relatively strong intermolecular hydrogen bonds C–H···O stabilizing the two-dimensional network. Two of them (6 and 8) are donated from the hydrogen atom located on C_α towards both the phosphonic and phosphonate groups, and the third one (7) is established between the ring C3 atom and the phosphonate group. So, an optimal use of the hydrogen-bond donor–acceptor capacity of molecule is executed in the formation of invariable molecular layers in **2**. The heterocyclic rings of the monolayers are arranged in stacks and van der Waals interactions (with mean H···H distance between the layers of

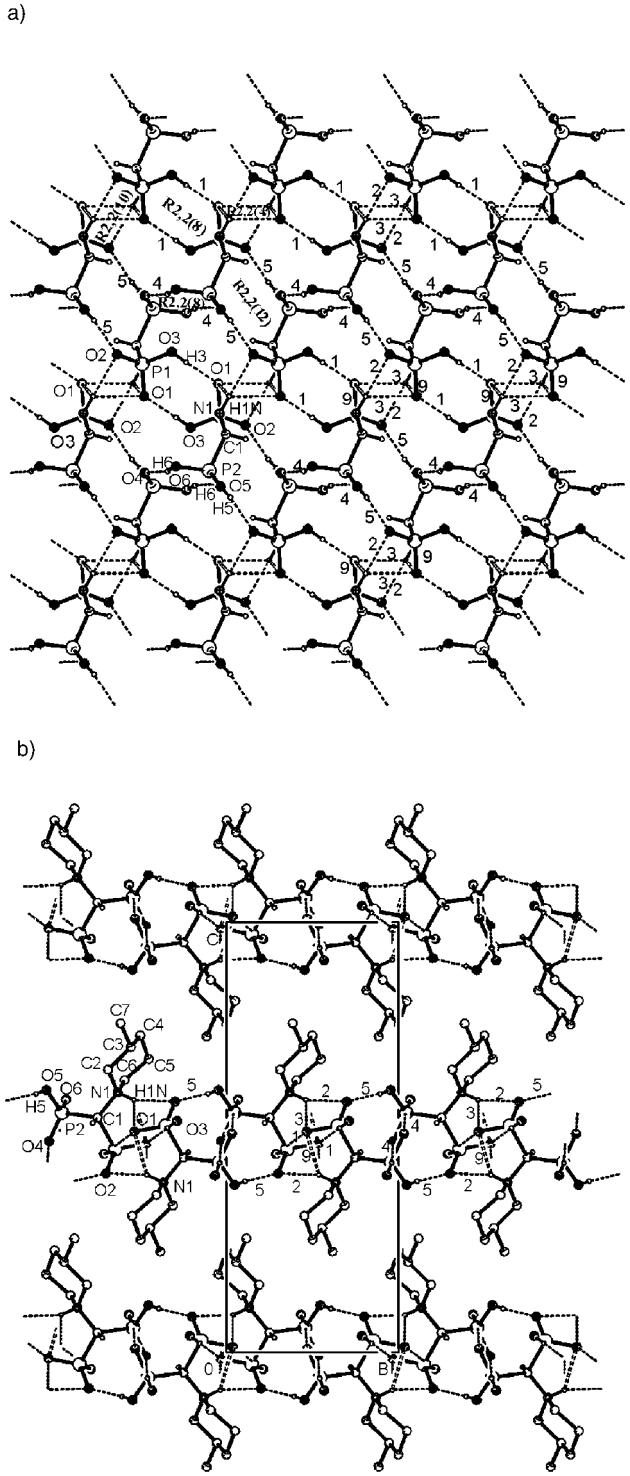

Figure 2. The hydrogen-bonded dimers of **2** (formed by 1 and stabilized by intramolecular hydrogen bonds 9, 10, and 11) are organized into (001) molecular monolayers with a hydrophilic interior and hydrophobic exterior: a) a view of the two-dimensional hydrogen-bonded network formed by multiple intermolecular hydrogen bonds 2, 3, 4, and 5. The heterocyclic rings and the stabilizing interactions 6, 7, and 8 are omitted from the picture; b) a side view of the monolayers demonstrating the heterocyclic ring arrangement (hydrogen atoms of the rings are omitted) and the interlayer relations. For the numbering of the hydrogen bonds see Table 3 and the text.

2.34 Å) hold adjacent screw-related monolayers in the third dimension.

*The crystal network of **3***: The movement of the methyl group from 3- to the 4-position leads to substantially modified molecular organization. A consideration at molecular level reveals that the strain between the methane-1,1-diphosphonic portion and the heterocyclic ring becomes somewhat relaxed, since only a single C2–H21···O4 bond (12) is established between the ring and the phosphonic group in addition to N1–H1N···O1 (11), common for all studied crystals (Figure 1b). Similar to **1** and **2**, the dimeric units are formed through the strong phosphonate–phosphonate interaction (O3–H3···O1, assigned as 1). However, unlike **2**, the extension of the dimers into molecular ribbons along the *a* direction is executed only by a single N1–phosphonate hydrogen bond (2). The one-dimensional network incorporates three ring motifs: two of them, R2,2(8) and R2,2(10), are generated by single hydrogen bonds (1 and 2, respectively), whereas the third one R2,2(4) arises from a combination of the intra- and intermolecular N1···O1 hydrogen bonds 2 and 11 (Figure 3a). Similar to **1** and **2**, the phosphonic groups are aligned on both sides of the ribbons and do not participate in the ribbon formations. However, the topology of the substituent prevents a close approach between neighboring ribbons and effectively disables any inter-ribbon hydrogen-bond and layer formation. Three symmetry independent water molecules serve as space fillers and hydrogen-bond linkers between the ribbons. Two of them, W1 and W3, stabilize and interweave the screw-related ribbons (through 3, 4, 7, 9). The third one, W2, also cross-links the molecular ribbons (through 6 and 8) and additionally accepts two more hydrogen bonds (5 and 10) from W3 and W1 in order to establish water bridges between the ribbons completing the three-dimensional network (Figure 3b). The heterocyclic portions of the molecules are arranged in the large hydrophobic channels (along the *a* direction) encircled by pairs of screw-related chains.

*The crystal network of **4***: The substituent group placed at the C2 atom in the ring is expected to interfere strongly with the methane-1,1-diphosphonic portion of the molecule. The three bulky groups, equidistantly positioned around N1, tend to stay as far as possible away one from another. This prevents the axial proton H21 at C2 to approach the phosphonate oxygen atoms, but enables the equatorial proton H62 at C6 to establish a new C_{ring}–phosphonate intramolecular hydrogen bond (11) in addition to the N–phosphonate and C_{ring}–phosphonic bonds (9 and 10, respectively) observed in **1**–**3**. The formation of C–H···O bonds to both P1 and P2 additionally stiffens the molecular conformation in **4** and **5**. However, the ethyl group, in contrast to the methyl one, is more apt to accommodate the requirements of the extended network established between the methane-1,1-diphosphonic portions of the molecules. Therefore, the one-dimensional arrangement in **4** resembles that in **3**. Phosphonate–phosphonate resonance-assisted and N–phosphonate

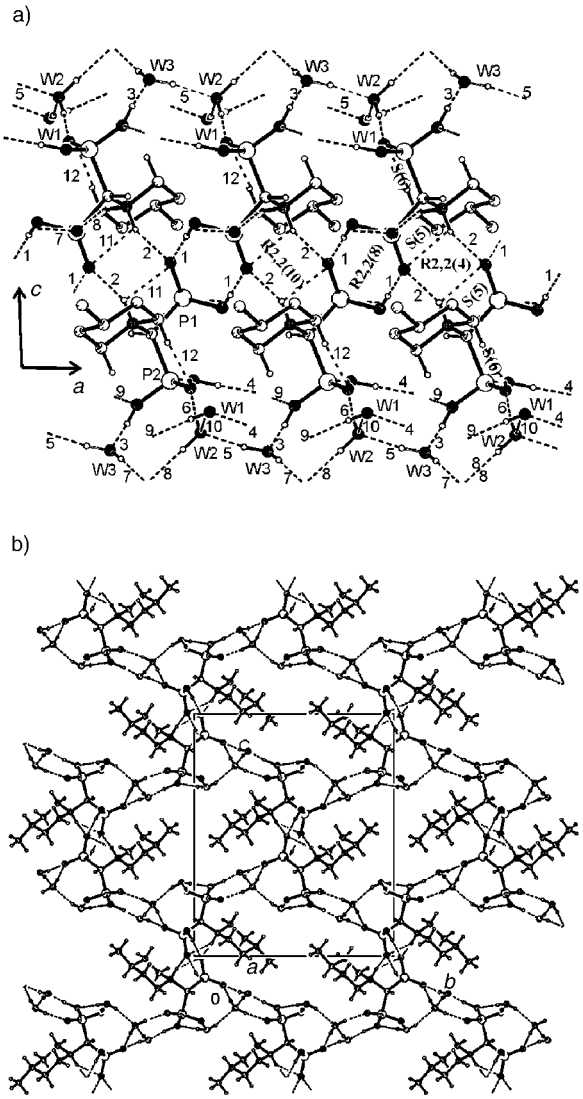

Figure 3. The hydrogen-bonded ribbons in **3** are mediated by three water molecules in order to form the three-dimensional hydrogen-bonded network: a) a view of the molecular ribbons demonstrates that only the phosphonate portions of the molecules **3** are used in the one-dimensional hydrogen-bonded extensions. The phosphonic portions, arranged from both sides of the ribbons are hydrogen bonded explicitly to the water molecules, that prevent the formation of molecular monolayers; b) a view along the ribbons envisaging the water bridges between the ribbons and the arrangement of the heterocyclic rings in the hydrophobic channels.

charge-assisted interactions (1 and 2) are used for ribbon formation in the *a* direction (Figure 4a). The phosphonic–phosphonate charge-assisted hydrogen bond O5−H5···O1 (3) links the neighboring ribbons into molecular monolayers (001). However, unlike **2**, in which all available hydrogen-bond donors and acceptors are used in hydrogen bonds inside the monolayer, some of the oxygen sites in **4** are inaccessible for intralayer hydrogen-bond formation. This generates large empty chambers between the ribbons of the molecular layers in **4**. For dense-packing reasons the crystal network incorparates one water molecule, which serves as

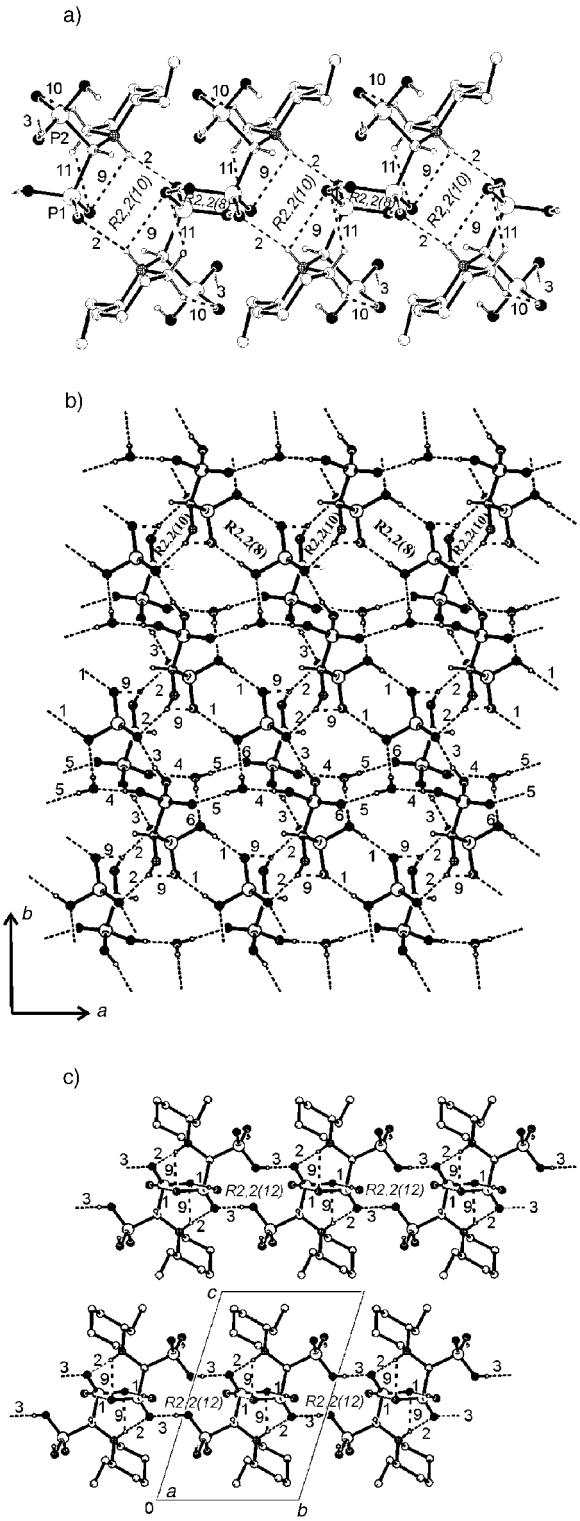

Figure 4. The one-, two-, and three-dimensional molecular arrangement in **4**. a) The molecular ribbon. b) The molecular layer. The water molecules in **4** are arranged inside the molecular layer traversing back and forth the empty spaces between the ribbons and forming water paths (tapes) parallel to the ribbons. The heterocyclic rings (omitted on the picture) are arranged in the exterior of the monolayer and fit in the pockets close between the molecular and the water tapes. c) A side view of two neighboring monolayers. The water molecules and the hydrogen atoms of the rings are omitted.

space filler and provides additional hydrogen-bond sites inside the layers. Water–phosphonate interactions (5) traverse the ribbons, whereas the phosphonic–water and water–phosphonic interactions (4 and 6) contrive water bridging tapes that are parallel to the molecular ribbons (Figure 4b). The rings protrude out of the layers and are arranged between them with the ethyl groups maximally deviated from the hydrophilic portion of the molecule (torsion angle N1-C2-C7-C8 of −157.8(2)°) so as to embed in the hydrophobic exterior (Figure 4c).

The crystal network of ***5***: The replacement of the ethyl group with the rigid methyl group extremely complicates the hydrogen-bonded network, and the comprehension of the molecular organization in **5** has been a challenging task for variety of reasons. The asymmetric unit of the crystal is composed of two independent molecular entities (assigned as A and B) (Figure 1d), which lead to an approximate screw rotation. This pseudosymmetry[12] is rationalized as a conflict between the hydrogen-bonding requirements and the need for optimal packing. Unlike the ethyl moiety, the methyl group is not able to align along the ring in order to escape the close approach of the methane-1,1-diphosphonic portion. The formal asymmetric dimeric unit A–B is formed through a strong pseudosymmetrical hydrogen bond O2B−H2B···O5A (1) by means of a D motif instead of the common R2,2(8). The molecular subunits are stabilized through eight hydrogen bonds: assigned as 15, 16, and 17 in A and 18, 19, 20, 21, and 22 in B. Intramolecular contacts are established between the methyl substituent and the phosphonate groups in both independent molecular units. Two more C−H···O bonds (23 and 24) traverse the independent units and contribute to the A-B formation in addition to 1. Three different hydrogen bonds (2, 3, and 4) extend the A–B entities into molecular ribbons along the *a* axis (Figure 5a). Four R2,2(10) ring motifs are generated in the ribbons by means of hydrogen-bond pairs 2–4, 3–4, 1–18, and 1–20, and two more ring motifs R2,2(12) are formed from a pair combination of 2–3 and 18–20. Two N−H···O bonds (5 and 6) link neighboring glide-related ribbons in order to form undulate molecular monolayers (001) with a hydrophilic interior and a hydrophobic exterior (Figure 5b). The heterocyclic rings, organized in the nanosized holes, protrude from the layer. The methyl groups point towards the interior rather than the exterior of the layer. This may be attributed to the hydrogen bonds (17 and 22) established between the methyl and the phosphonic/phosphonate

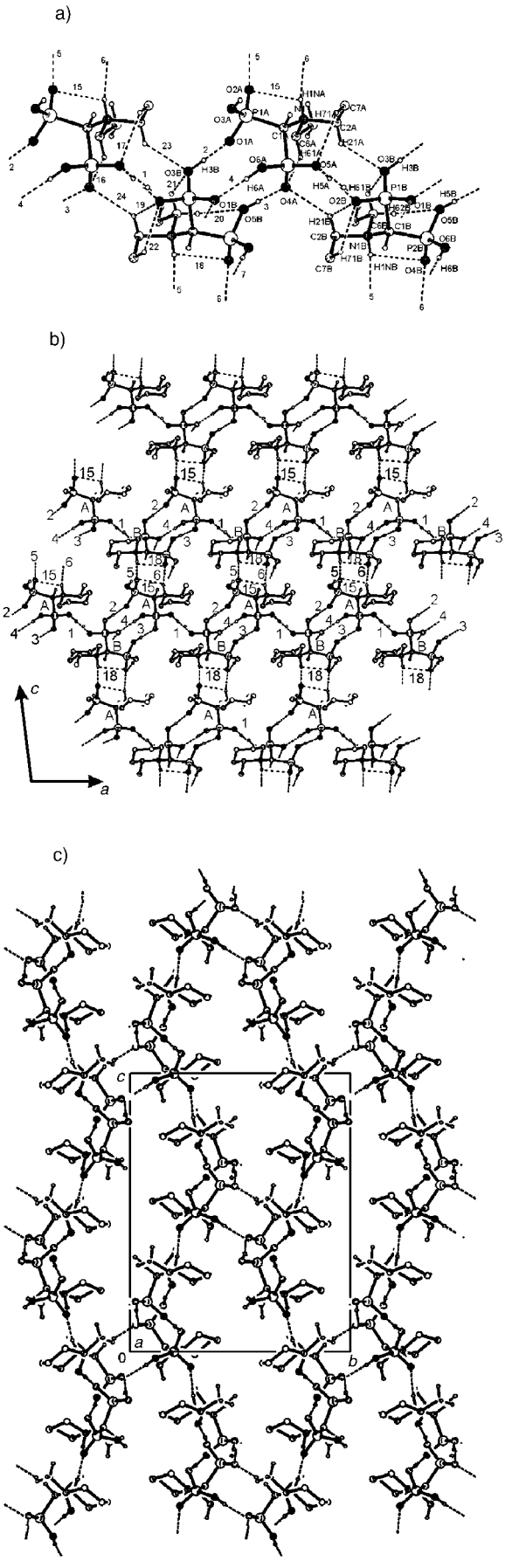

Figure 5. The one-, two-, and three-dimensional solid-state molecular organization of **5**. a) A presentation of the formal molecular ribbons formed by the independent dimeric units A–B (the heterocyclic rings of the molecules are omitted). b) View of the formal molecular monolayers (010). The rings are locked in the spaces between the ribbons. c) A side view of four molecular monolayers revealing the interlayer hydrogen-bond relations. The giant empty spaces generated between the layers are filled by the water molecules (omitted on the picture) that serve as additional hydrogen-bond agents between the layers.

groups. Markedly, the methyl hydrogen atoms H71A and H71B approach exactly the oxygen sites (O5A and O2B) already engaged in the disordered hydrogen bond 1. Therefore, the character of the proton disorder in 1 is presumed to be dynamic, resulting from the movement of the methyl group. Reasonably, the proton H2B(H5A) becomes disordered between the oxygen sites of the asymmetric units A and B (with an occupancy factor 63% to O2B and 37% to O5A).

Another way to disentangle the two-dimensional network in **5** is to consider the ribbon formations in the [101] direction (generated by phosphonate–phosphonate and N–phosphonate interactions as in crystals **1**–**4**; see Figure 5b), that are connected by the pseudosymmetrical hydrogen bond 1. However, the fluctuant repulsion and attraction effects between the librating methyl group, the H2B(H5A) proton sites, and the O2B and O5A oxygen sites prevent the close inversion relation between the ribbons and the generation of the R2,2(8) motif observed in **1**–**4**. Instead of this, the molecules use translation and glide-reflection relations between two independent molecular units A–B, which almost have screw related symmetry. The water disorder observed in **5** may also be explained by the dynamic behavior of the system. Such a delineation of the molecular organization is reasonable with respect to the similar solution behavior of **4** and **5**. Indeed, there is no difference between A and B molecules in solution and the doubling of Z′ in the crystal is only the way in which the molecules choose to accommodate spatial demands of the substituent with the directional dictates of the intermolecular interactions. The heterocyclic rings, arranged to form stacks along [101] direction, are embedded in the hydrophobic channels generated between the monolayers. The glide relationship inside the layers allow for a connection only between B subunits in the interlayer region. The R2,2(8) motifs generated between the neighboring monolayers through bond 7 are placed at a distance of 18.688 Å along the *c* axis (Figure 5c). Three water molecules fill in the large pockets of the interlayer region. Two of them, W2 and W3, are disordered with an occupancy of less than 50%.

Spectroscopic characteristics: The complete assignments of the room-temperature ^{1}H and ^{13}C NMR spectra of compounds **1**–**5** are presented in Table 4. The positions of the resonances of the piperidine ring have been determined with the aid of the ^{1}H-^{1}H COSY, ^{13}C–^{1}H HMQC, and DEPT 135 experiments, and verified by iteration of each ^{1}H NMR spectrum. The number of resonances in the spectra is in accordance with the symmetry considerations. The presence or absence of large vicinal proton–proton coupling constants has been used as a diagnostic tool for distinguishing the axial and the equatorial protons. The magnitudes of the diaxial ^{3}J(H,H) coupling constants ranging between 13.6–11.5 Hz show that the piperidine ring in **1**–**5** predominantly adopts a chair conformation in solution.

The characteristic feature of both the ^{1}H and the ^{13}C NMR spectra of compounds **1**–**5** is a triplet (doublet of doublets) arising from the coupling of the $C_{\alpha}H$ proton or carbon atoms with the ^{31}P nuclei of the phosphonate groups.[9] The binding of the methane-1,1-diphosphonate portion to the piperidine nitrogen atom shields the resonances of the nearest C2 and C6 ring carbon atoms relative to those of the parent piperidine.[13] Similarly, the signals of H2 and H6 in the corresponding ^{1}H NMR spectra are strongly shielded and therefore easy to recognize.

The comparison of the ^{13}C NMR spectra of **2**–**5** with that of **1** shows that the replacement of the hydrogen atom with an alkyl group in the piperidine ring exerts downfield shifts (~6–8 ppm) on the resonances of the carbon atoms at α- and β-positions with respect to the substituent. The most pronounced shielding (11.73 ppm) is detected on the alkylated C2 carbon atom of **4**, whereas the C3 carbon atom in the β-position versus the 2-ethyl group is less affected ($\Delta\delta$ = 4.48 ppm), when compared to **2**, **3**, and **4**. A shielding due to

Table 4. ^{1}H, ^{13}C, and ^{31}P NMR spectral data [ppm] for compounds **1**–**5** in D_2O at 300 K.

	$C_{\alpha}H$	H2		H3		H4		H5		H6		CH_2	CH_3
		ax	eq	ax	eq	ax	eq	ax	eq	ax	eq		
1	3.52 (19.2)[a]	3.59	3.52	1.70	1.89	1.38	1.71	1.70	1.89	3.59	3.52	–	–
2	3.55 (19.6)	3.22	3.42	1.83	–	1.05	1.73	1.70	1.88	3.50	3.50	–	0.86
3	3.55 (19.2)	3.61	3.50	1.38	1.86	1.60	–	1.38	1.86	3.61	3.50	–	0.85
4	3.81 (20.8)	3.76	–	1.56	1.96	1.44	1.75	1.61	1.87	3.47	3.72	1.63; 1.83	0.86
5	3.84 (21.3)	3.86	–	1.65	1.90	1.46	1.72	1.62	1.89	3.47	3.78	–	1.33

	^{13}C								^{31}P
	$C_{\alpha}H$	C2	C3	C4	C5	C6	CH_2	CH_3	
piperidine[13]		47.5	27.2	25.2	27.2	47.5	–	–	–
1	62.84 (120.4)	54.41 (4.8)	24.03	20.93	24.03	54.41 (4.8)[a]	–	–	7.12
2	62.71 (122.1)	59.62 (4.1)	30.41	29.55	23.65	53.83 (4.1)	–	17.93	7.16
3	62.41 (121.5)	54.08 (4.8)	31.94	27.90	31.94	54.08 (4.8)	–	20.29	7.20
4	57.25 (126.8) 55.71 (126.4)	66.14 (5.5)	28.51	21.97	23.42	54.01	24.09	7.64	8.52; 6.17
5	57.89 (126.0) 56.33 (125.3)	61.76 (5.6)	32.27	22.09	24.02	53.52	–	17.73	8.60; 6.19

[a] J(P,H) and J(P,C) [Hz] experimental values in parentheses.

the 2-alkyl substitution is also observed for the $C_\alpha H$ proton signals of **4** and **5**, which demonstrate a downfield shift of approximately 0.3 ppm relative to $C_\alpha H$ of **1–3**.

In order to comprehend the solution behavior of compounds **1–5**, their NMR spectra have been monitored over a broad range of pH. The studied compounds represent a family, in which each of the phosphonate (PO_3^{2-}) groups is capable of accepting two protons and the heterocyclic nitrogen atom one proton. Although in solid state all compounds exist in the zwitterionic form [H_4L] (Figure 1); the dominating form in solution is [H_3L]$^-$. This is due to the fact that the PO_3H_2 group is strongly acidic and dissociates well below pH 2. Therefore, as much as three protons (one proton from each of the phosphonate groups and one from the nitrogen atom) can potentially be released in the measurable pH range. Figure 6 displays the ^{1}H NMR titration

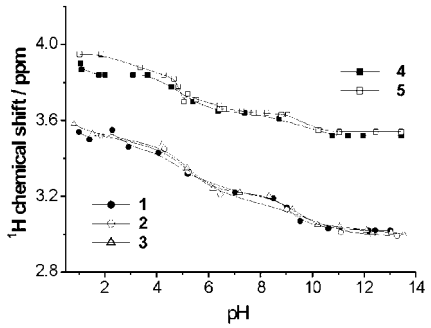

Figure 6. ^{1}H NMR chemical shifts of the methine $C_\alpha H$ proton as a function of pH for compounds **1–5**.

curves for $C_\alpha H$ proton of compounds **1–5**. The steep upfield shifts of the resonances clearly demonstrate that only two subsequent deprotonations take place from the two PO_3H^- groups. Similar to other aminomethane-1,1-diphosphonic acids, the release of the proton from the more acidic PO_3H^- group is separated by nearly four pK units from that of the less acidic one.[14] The proton located on the piperidine nitrogen atom is not removed even in very strong alkaline solutions as evidenced from the spectra. Therefore, the intramolecular N1–H1N···O (phosphonic or phosphonate) hydrogen bond, observed in the crystals **1–5**, is apparently an inherent property of these compounds and is retained also in solution. To confirm the conclusions drawn from the ^{1}H NMR spectra, the corresponding ^{31}P NMR titrations were also performed (Figure 7). In the spectra of compounds **1–3** (Figure 7a), both phosphonate moieties result in a single peak, which is slightly sensitive ($\Delta\delta \sim 0.5$ ppm) to the variations in their protonation states. This additionally proves that the heterocyclic nitrogen atom remains protonated over the whole studied range of pH, since otherwise a significant downfield shift of the ^{31}P resonance should be observed in alkaline solutions.[15]

As far as **4** and **5** are concerned their pH dependences of the $C_\alpha H$ proton chemical shifts versus pH are quite similar to those of **1–3**. However, their ^{31}P NMR spectra are significantly different (Figure 7b). There are two distinct pH areas, (pH < 6 and pH > 8), in which the two independent resonances demonstrate exactly the opposite trend for the changes of the chemical shift versus pH. On the other hand, in the intermediate pH range 6→8 the signals thoroughly coalescence in **4** and are very close in **5**. Taking into account that the approximate pK_a values for a dissociation of the proton from the PO_3H^- groups are 4.5 and 8.5 (Figure 6), the largest differences in the ^{31}P chemical shifts correspond to pH ranges in which both phosphonate groups remain monoprotonated or in which both exist predominantly as diprotonated PO_3^{2-} forms. The corresponding ^{13}C NMR spectra of **4** and **5** display narrow lines in the acidic and alkaline solutions, whereas in the pH range 6→8 the signals are significantly broadened. In addition, only minor changes are detected in the ^{31}P spectra performed for acidic and alkaline solutions with heating of the samples up to 350 K. On the other hand, the single resonance detected in the ^{31}P NMR spectra of **4** in the pH range between 6→8 splits upon cooling into two lines, which suggests a dynamic behavior of the compound.

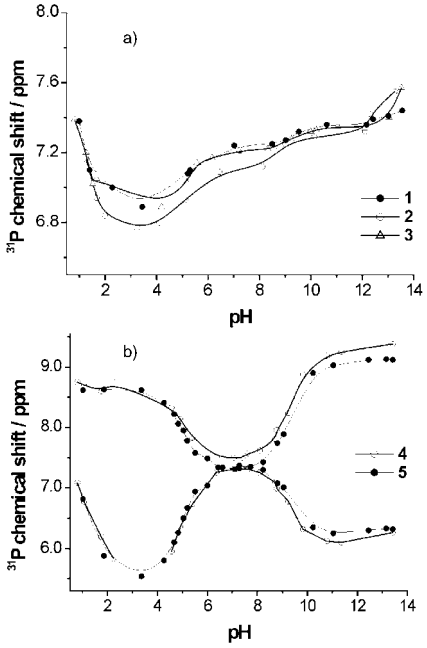

Figure 7. ^{31}P NMR chemical shifts as a function of pH: a) compounds **1–3**; b) compounds **4** and **5**.

Solution properties of compounds 1–5: The structural analysis (Table 3) has revealed the strong inclination of the molecules **1–5** for self-recognition and dimer formation through phosphonate–phosphonate and/or phosphonic–phosphonic interactions between alike sites. The entire crystal is built up by dimer units that form according to the conventional space group symmetry. However, the periodical distribution of the noncovalent bonds between the dimers are different, essentially depending upon the topology of the substituent. Although the priority of hydrogen bonds with respect to

their strength (provided that the contact distance is a strength-reflecting factor) can be argued, it seems reasonable to anticipate that the hydrogen bonding between the monoprotonated sites initiates the molecular organization in solution, gradually eliminating other less preferred formations. This is justified by the fact that this binding, which does not allow for multiple choices, reduces the possible combinations and minimizes the wrong recognitions. Indeed, in all crystals **1**–**5**, the phosphonate–phosphonate $P1O_3H^-$–$P1O_3H^-$ interaction is used for dimer formation. The phosphonic–phosphonic and the N–phosphonate hydrogen bonds obey the symmetry requirements for ribbon formation. The phosphonic–phosphonate interactions, used in the two-dimensional arrangement, intermingle the $P2O_3H_2$ and the $P1O_3H^-$ sites of the ribbons and generate bigger hydrogen-bond motifs.

Considering the crystal disintegration upon dissolution as a process opposite to crystal formation, we may be able to anticipate some of the solution aggregation forms. The stepwise disruption of the network and the gradual reduction of the long-range symmetry lead to smaller molecular assemblies, stable under certain conditions in solution. The nondirectional packing forces and the weak intermolecular C–H···O hydrogen bonds, stabilizing the network, evidently are the first to be released. The multiple strong hydrogen bonds established between the $P2O_3H_2$ and $P1O_3H^-$ sites break stepwise, and this process essentially depends upon pH and other external conditions in solution. The gradual release of protons upon increasing pH leads to enhanced molecular motions and conformational freedom. This correlates well with the NMR results.

Conformation dynamics: The whole set of intramolecular motions in six-membered saturated azacycles includes three different types of motions: ring inversion (RI), nitrogen inversion (NI), and rotation around the C–N bond (R).[16] However, the nitrogen inversion is not allowed when nitrogen is tetrasubstituted and only isolated RI and R processes or a concerted RI/R process are in principle expected to determine the stereodynamics in **1**–**5**.

In **1**–**3** the only reliable constrain on the molecular conformation in solution is the intramolecular N1–H1N···O1 hydrogen bond. Therefore, the molecules **1**–**3** may potentially convert between two chair conformations **A** and **B**. Additionally, each of the conformational isomers **A** and **B** may exist as a mixture of three different rotamers, provided that some movement's freedom around the exocyclic C1–N1 bond is allowed. This is demonstrated in Scheme 1 for **1**, the simplest compound of the studied set.

The ring inversion in **1** is clearly evidenced in the ^{1}H 2D exchange (EXSY) spectrum showing the correlation peaks

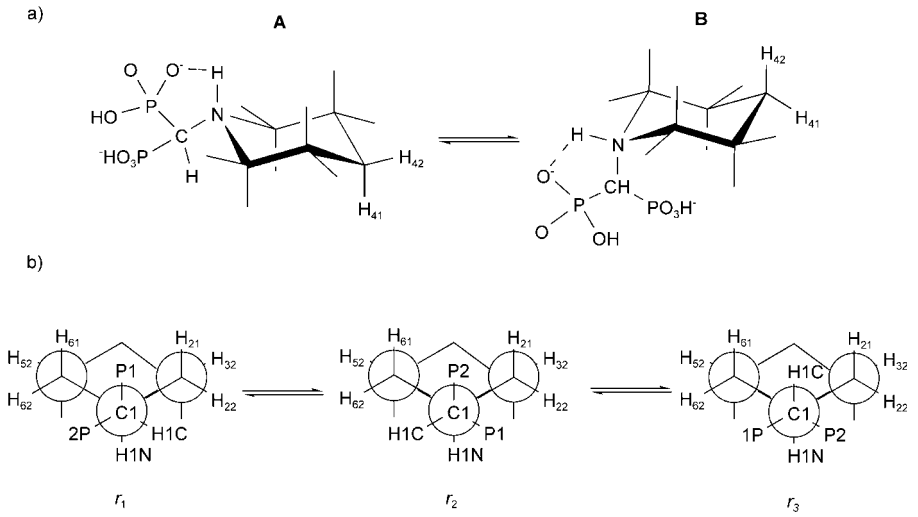

Scheme 1. a) The **A** and **B** conformers of **1** issued from the ring inversion. **A** corresponds to the isomer, that was experimentally found in solid state.[10] b) The Newman projections for the **A** conformer, with an assumption of staggered rotamers around the C1–N1 bond. The numbering is consistent with that of the crystals. The positions of P1 and P2 in r_1 correspond to those found in solid state.

issued from the exchange phenomena between $H4_{ax}$ and $H4_{eq}$ as well as $H3,5_{ax}$ and $H3,5_{eq}$. The cross peaks correlating $H2,6_{ax}$ and $H2,6_{eq}$ are less visible due to their close positions. The nonequivalence of the ring geminal protons, detected in the room-temperature ^{1}H NMR spectrum, is most likely connected with the steric impediment on N1. Although the bulk effects of the methane-1,1-diphosphonate moiety may also account for the increase of the rotational barrier, the room-temperature ^{31}P NMR spectrum of **1** displays only one resonance, which demonstrates that both phosphonate groups are equivalent (Table 4) and that the rotation is fast on the ^{31}P NMR timescale.

This behavior can be explained if the possible populations of the rotamers around the C1–N1 bond (Scheme 1, bottom) are taken into consideration. The ring movement around C1–N1 in r_1 and r_2 allows the protons on N and the closest C atoms to approach the oxygen atoms of the phosphonate group (P1 or P2) in order to form "dynamic" hydrogen bonds. This allows us to presume that both r_1 and r_2 are nearly equally populated and therefore can be considered as predominant rotameric forms in solution. Although the P1 and P2 oxygen sites in r_3 are equally accessible for the nitrogen proton, they are not accessible at all for the carbon protons; this seemingly makes this form less stable and less abundant in solution. Evidently, the rate of exchange between r_1 and r_2 is determined by the rate of reversible formation and breaking of the N1–H1···O(phosphonate) hydrogen bonds.

Some structure-dependent differences become evident when we compare the spectra of **2** and **3** with those of **1**. The most important one is the lack of chemical exchange between the geminal ring protons in the EXSY spectra of **2** and **3**, which shows that the inversion of piperidine ring is locked upon substitution in 3- or 4-position and only one conformer predominates in solution. The well-documented tendency of the ring substituents to adopt, whenever possible, equatorial positions,[16f,17] confirmed by the structures of the studied compounds, allows us to assume that both **2** and **3** adopt the **A** conformation in solution. Therefore, the stereodynamics of **2** and **3** is determined by the rotation around the C1–N1 bond concerted with the N1–H1···O(phosphonate) hydrogen-bond breaking/formation process. The rotation is fast on the ^{31}P NMR timescale, since similar to **1**, only one resonance is detected in the corresponding spectra. The equal values for ^{3}J(P,C2) and ^{3}J(P,C6) coupling constants found in all compounds **1**–**3** also confirm this (Table 4).

Differences dependent on the substituent and its position in the ring are reflected also in the ^{1}H NMR spectra measured versus temperature and pH. Heating the sample of **1** (Table 4) up to 350 K leads to coalescing of the lines for H2,6 and H3,5 and unusual broadening of the $H4_{ax}$ and $H4_{eq}$ signals. These effects can be explained by the ring dynamics concerted with the formation and breaking of inter- and intramolecular hydrogen bonds. The temperature rise accelerates the concerted ring inversion/rotation process (RI/R), which in turn accelerates the formation/breaking processes of the intramolecular N1–H1···O(phosphonate) and C–H···O(phosphonate) hydrogen bonds. On the other hand, the intermolecular hydrogen bonds also become more labile and can break with increasing temperature. No molecular aggregations are expected at high temperatures. The spectral behavior versus pH is very similar. The increase of pH from ~1 to 13 leads to a stepwise coalescence of the signals for the ring geminal protons in the order H2,6 > H3,5 > H4 with a complete averaging to single broad lines achieved at pH > 12. This can be explained with the gradual deprotonation of the phosphonate groups and the intermolecular hydrogen bonds breaking, leading to complete disintegration of any aggregation forms. Generally, the spectral changes with the temperature and pH are better visible for the protons very close to the N atom. This seems to correlate well with the ascending order of $\Delta\delta_{ae}$ values ($\Delta\delta_{ae}$: the chemical shifts difference between the geminal protons) for H2,6, H3,5, and H4 protons, namely 0.07, 0.19, and 0.33 ppm, found from the room-temperature spectrum (Table 4). The above experiments show the significant contribution of the rotation to the overall ring movement processes.

The ^{1}H NMR changes with temperature and pH observed for **2** and **3** are very conclusive for the gradual decrease of the rotational contribution to the ring dynamics, which is logical taking into account that the replacement of a ring proton for the bulkier Me group makes the heterocycle less flexible. The ring rigidity is essentially dependent upon the substituent's position and its possible interference with other steric impediments. So, in **3** the effect of the substituent is expected to be significantly less important than in **2**, since the Me group in the 4-position is pretty far from the methane-1,1-diphosphonate portion of the molecule. The experimental results are in excellent agreement with this reasoning. The $\Delta\delta_{ae}$ values in the room-temperature ^{1}H NMR spectrum of **3** are 0.11 ppm (H2,6) and 0.48 ppm (H3,5). Accordingly, the heating of the sample up to 350 K causes only the H(2,6) resonance to coalesce to a single line, whereas the signals for $H3,5_{ax}$ and H4 markedly broaden and $H3,5_{eq}$ remains unchanged. The increase of pH influences the spectra in more complex way. In particular, the signals for H2,6 start to broaden at the beginning, then coalesce at pH6→8, and finally reappear again as two resonances at pH > 8. This is accompanied by a gradual broadening of the H4 and $H3,5_{ax}$ resonances upon pH increase up to ~8, but the signals invert their trend at pH higher than 8. However, the ^{1}H NMR spectra of **2** display only narrowing of the signals for the closest H2 and H6 protons, and the other ring proton resonances remain almost unaffected by the pH or temperature changes. This feature indicates that the rotational movement around the C1–N1 bond, although being still fast on the ^{31}P NMR timescale, is significantly reduced in **3** and especially in **2**, relative to that in **1**. So, in contrast to **1**, only hydrogen-bond breaking/rotation/hydrogen-bond formation processes are responsible for the ring movement in **2** and **3**, and the rate of rotation in **2** is significantly reduced versus that in **3** and especially that in **1**.

The situation is significantly more intricate in **4** and **5**, since even under basic conditions some molecular aggregations are retained. Essentially, the dissolution processes of **4** and especially of **5** are different from that of **1**–**3**. For example for compound **4**, the release of the proton H6 upon dissolution leads to a destabilization of the layers, eventually to a discontinuation of the long-range periodicity, but not to a destruction of the two-dimensional molecular assemblies. Only after the second proton (H5) is released (at slightly acidic conditions) do the assemblies break into smaller molecular aggregations (organized around the primary dimers), which eventually have short-range arrangements due to the N–phosphonate interactions. The unrestrained $P2O_3^{2-}$ group is free to rotate around the C1–P2 bond. The monoprotonated $P1O_3H^{-}$ group, constrained in the dimer ring motif, can rotate around the C1–P1 bond only in a concerted way embracing the whole dimer, which in turn harms the rotation around the C1–N1 bond. The only possible conformational change in the dimer is a simultaneous flipping of both heterocycles in two opposite directions. The dimers (R2,2(8)) break after the release of H3. However, even at very basic conditions, certain "dynamic" formations may still exist in solution due to interchangeable N–phosphonate interactions. The solution behavior of compound **5** is very similar to that of **4**.

The **A** conformer is considered to be the predominant form upon dissolution also in **4** and **5**. This is evidenced in the lack of exchange peaks between the ring geminal protons in the EXSY spectra and in the narrowing of the

^{1}H NMR resonances upon temperature increase. The $\Delta\delta_{ae}$ values for H3, H4, H5, and H6 protons (0.40, 0.31, 0.26, 0.25 ppm in **4** and 0.20, 0.26, 0.27, 0.31 ppm in **5**) are similar and remain almost constant over the whole studied pH range. This presumably reflects the lower flexibility of the piperidine ring in **4** and **5** relative to **1–3**.

In view of the above considerations it becomes clear that the chemical environment of the two phosphonate groups in **4** and **5** is different even in solution. So, the different resonances detected at low and high pH ^{31}P NMR spectra (Figure 7b) are attributed to different phosphonate groups. The high-field resonance (at pH < 6) is assigned to the $P2O_3H^-$ group, which is deprotonated first. The lower field signal is assigned to the $P1O_3H^-$ group, which is constrained in the hydrogen-bonded dimer. The nonequivalence of P1 and P2 is also reflected in the ^{13}C NMR spectra (Table 4). The C_α carbon atom displays two separate doublets (instead of an averaged triplet) observed in the whole measurable pH range, which is affected by the coupling to the nonequivalent P1 and P2 atoms. Essentially, the ^3J(P,C) coupling constant of approximately 5.5 Hz is observed for only one carbon atom, C2.

The very unusual ^{31}P NMR spectral behavior can be explained with the steric effects of three equidistant bulky groups around the heterocyclic N-atom (the alkyl and the two phosphonate groups) and the consequences for the molecular motion. For example, in **5** the H1N proton preferably forms intramolecular hydrogen bond with the less acidic $P1O_3H^-$, retaining the **A** conformer in acidic conditions. However, both phosphonate groups tend to stay far away from the alkyl substituent and the axial proton H21 (on C2) cannot approach any of the oxygen atoms. Instead of this, the equatorial proton H61 (on C6) binds internally to the $P1O_3H^-$ group and the axial proton H61 to $P2O_3H^-$. A crucial moment is the increase of a negative charge on P2 after a proton release upon rising pH, which makes the $P2O_3^{2-}$ group more attractive for the nitrogen proton H1N. However, the P2 oxygen atoms still remain inaccessible for the nitrogen proton, due to constrains imposed by the crossed hydrogen bonds donated from C6 towards both P1 and P2. So, the only way for H1N to form a hydrogen bond towards P2 group is a conformational change through a flipping of the ring (Scheme 2).

In the pH range 6→8 **A** and **B** are likely to occur in an approximate 1:1 ratio. The contribution of both conformers

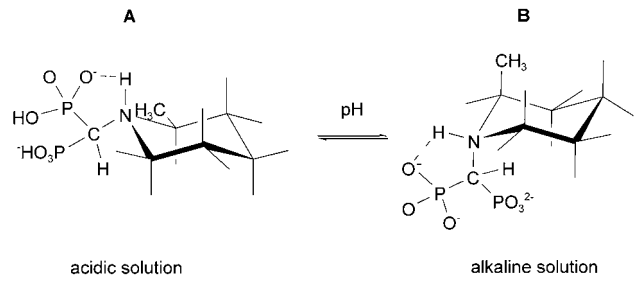

Scheme 2. The pH switched conformations of **4** and **5**.

may explain the existence of one averaged ^{31}P NMR signal for the phosphonate groups in **4** and the appearance of two very close resonances in the spectrum of **5**. The dynamic equilibrium in this range is confirmed by the separation of the ^{31}P NMR signal of **4** into two peaks on cooling to 283 K. Accordingly, the room-temperature ^{13}C NMR spectra in the pH range 6–8 demonstrate a markedly broadened resonances for all carbon atoms, including C_α, except for the CH_2 signal of the ethyl group. A noticeable broadening is observed also in the ^{1}H NMR spectra. No EXSY cross peaks are detected in the pH range 6→8 under the conditions of the experiment. All resonances in both ^{1}H and ^{13}C NMR spectra undergo further narrowing on going to higher pH values. This presumably results from the conformational switching from **A** into **B** form, with a consequent predominance of the **B** conformer at the end of titration.

Conclusion

We have demonstrated that combination of solid-state structural and solution NMR methods is helpful for uncovering structural and conformational problems in the studied compounds. We have shown that nature and topology of the substituent significantly account for the recognition and aggregation preferences and, therefore, for the solution behavior. All compounds (except **3**) form molecular layers; however, the intra- and interlayer organization in **1**,**2** and **4**,**5** differs. The existence of these different forms also predominates upon dissolution. The crystal structure of **3** is intermediate between **1**,**2** and **4**,**5**. Additionally, we have revealed the substantial role of the intra- and intermolecular hydrogen bonds, not only for the organizational processes in solution and solid state, but also for the conformation dynamics in solution.

We experimentally proved that ring-inversion/rotation concerted with the N1−H1···O(phosphonate) hydrogen-bond breaking/formation process leads to a mixture of interconverting conformers (**A** and **B**) in solutions of **1**. On the other hand, placement of an alkyl group in the ring prevents the inversion and leads to a predominance of the **A** conformer in solutions of **2** and **3**. The concerted N1−H1···O(phosphonate) hydrogen-bond formation/rotation/N1−H1···O(phosphonate) hydrogen-bond dissociation process is significantly influenced by the substituent and its position in the ring. The rate of rotation decreases in the following order **1** > **3** > **2**. The rotation process in **4** and **5** is disabled, which makes them less flexible than **1–3**. The influence of pH on the conformation dynamics in **4** and **5** is evidenced as well. Both compounds can exists as an **A**⇌**B** mixture with equilibrium shifted to the left in acidic solutions and to the right in alkaline solutions.

If now we try to correlate the biological activities of **1–5** documented by Oldfield[11] with the results of our studies they seem to be more comprehensive. Generally, compounds existing as monomolecular forms, with a predominance of one conformer in solution, are considered to be

more effectively bound by the receptor. The binding capacity and the resulting receptor response are significantly reduced if variable conformations and/or aggregational forms are present. Evidently, external factors (like pH) can significantly influence the existing equilibria and, therefore, play a substantial role for the biological activity of the compound. For example, compound **3**, the most potent compound in the series, is most labile among the studied substituted compounds. Additionally, the monomolecular forms of only one conformer predominate already at neutral pH conditions. In contrast, the conformational equilibria for the most rigid compounds **4** and **5** are pH dependent and certain small aggregates are the prevailing formations even at basic conditions. This might be one of the reasons for their significantly lower potency relative to **1**–**3**. The twofold higher potency of **4** versus **5** may be explained with the relatively better adaptability of the substituent group.

Experimental Section

Sample preparation: The piperid-1-ylmethane-1,1-diphosphonic acids were synthesized according to a literature procedure[18] in the reaction of appropriate amines with ethyl orthoformate and triethyl phosphite, followed by acid hydrolysis of the obtained esters. This reaction afforded the required compounds in satisfactory yields (37–64%). The single crystals of **2**, **3**, **4**, and **5** were grown from water at room temperature by using the slow evaporation method.

Crystal structure determination: The X-ray diffraction data collection was performed at 100 K on a KUMA KM4 CCD four-circle diffractometer[19] equipped with an Oxford Cryosystem Cooler by using graphite-monochromated $Mo_{K\alpha}$ radiation, $\lambda = 0.71073$ Å. The crystal structures were solved by direct methods by using the SHELXS97 program[20] and refined by full-matrix least-squares technique by using SHELXL97.[21]

All H atoms in the structures of **2**–**4** were found in the difference Fourier maps and were refined isotropically except for H22 in **2**, which was refined with U_{iso} equal to U_{eq} of the parent C2 atom.

All nitrogen and oxygen H atoms in **5** were found in the difference Fourier maps and refined with $U_{iso} = 1.2\,U_{eq}$ of the proper O or N atoms. The hydroxyl O5A–H5A and O2B–H2B distances were constrained to 0.86 Å. Additionally, the H3W···H4W, H5W···H6W, and H5W···H7W distances were constrained to 1.43 Å. The site occupation factors for the water molecules in **5** were 1 for W1 (O1W, H1W, H2W) and 0.5 for W2 (O2W, H3W, H4W). The oxygen and the hydrogen atoms of W3 were observed at positions O3WA, O3WB, H6W, H7W (with s.o.f. = 0.5) and H5W (s.o.f. = 1). All C-bonded H atoms, except those of the methyl groups, were included from the geometry (using one of the AFIX instructions) and refined with $U_{iso} = 1.2\,U_{eq}$ of the parent C atoms.

The XP package[22] was used to generate the molecular drawings. The computer program Platon[23] was used for analysis and graphical presentation of the hydrogen bonding patterns.

CCDC-235483 (**2**), CCDC-235484 (**3**), CCDC-235485 (**4**), and CCDC-235486 (**5**) contain the supplementary crystallographic data for this paper. These data can be obtained free of charge from The Cambridge Crystallographic Data Centre via www.ccdc.cam.ac.uk/data_request/cif.

NMR measurements: NMR spectra were recorded on a Bruker Avance DRX-300 spectrometer operating at 300.13 MHz for ^{1}H, 75.46 MHz for ^{13}C and 124.50 MHz for ^{31}P, and some 1D ^{1}H NMR spectra on a Bruker Avance DRX-500 spectrometer operating at 500.13 MHz; $T = 300$ K, unless otherwise noted. The chemical shifts are given relative to 85% H_3PO_4 (^{31}P) and $SiMe_4$. All downfield shifts are denoted as positive. The standard Bruker programs were used to perform 1D experiments.

The 2D experiments were carried out with the following parameters: 1) [^{1}H–^{1}H] COSY spectral width 1800 Hz in both dimensions, 512 F1 increments, relaxation delay of 2 s, a 512 × 2048 data matrix, and 16–32 scans for each FID; a sine weighting function was applied prior to Fourier transformation; 2) [^{13}C–^{1}H] HMQC with 256 F1 increments, relaxation delay 2 s and Bird delay 650 ms, a 256 × 1024 data matrix, and 24 scans for each FID; a $\pi/2$ shifted sine-squared weighting function was applied prior to Fourier transformation; 3) NOESY (EXSY) spectra were acquired in the phase-sensitive mode by using time proportional phase incrementation (TPPI), mixing time $t_m = 500$ ms→1 s, relaxation delay 4 s, spectral width 2400 Hz in both dimensions, 512 F1 increments, a 512 × 2048 data matrix, and 16 scans for each FID; a $\pi/2$ shifted sine-squared weighting function was applied prior to Fourier transformation.

The variable-temperature measurements covered the temperature ranges 283–350 K (^{31}P) for **4**, **5** and 300–350 K (^{1}H) for **1**–**5**.

The samples for NMR studies were prepared in deuteriated water. The concentration of the samples was 1×10^{-1} mol dm^{-3} for ^{13}C and 2×10^{-2} mol dm^{-3} for the ^{1}H and ^{31}P titration measurements. The pH was measured using a Radiometer pHM 83 instrument equipped with a Mettler Toledo INLAB 422 combined electrode and is given as meter ridings without correction for pD.

Acknowledgement

The financial support from the Polish State Committee for Scientific Research (Project PBZ-KBN-060/T09/2001/14) is thankfully acknowledged.

[1] a) D. E. Hughes, M. Mian, D. F. Guilland-Cumming, R. G. G. Russel, *Drugs Exp. Clin. Res.* **1991**, *17*, 109–114; b) G. A. Rodan, T. J. Martin, *Science* **2000**, *289*, 1508–1514; c) M. J. Rogers, S. Gordon, H. L. Benford, F. P. Coxon, S. P. Luckman, J. Mönkkönen, J. C. Frith, *Cancer* **2000**, *88*, 2961–2978; d) L. Widler, K. A. Jaeggi, M. Glatt, K. Müller, R. Bachmann, M. Bisping, A.-Ruth Born, R. Cortesi, G. Guiglia, H. Jeker, R. Klein, U. Ramseier, J. Schmid, G. Schreiber, Y. Seltenmeyer, J. R. Green, *J. Med. Chem.* **2002**, *45*, 3721–3738.

[2] a) M. J. Rogers, J. C. Frith, S. P. Luckman, F. P. Cox, H. L. Benford, J. Mönkkönen, S. Auriola, K. M. Chilton, R. G. G. Russell, *Bone* **1999**, *24*, 73s–79s; b) E. van Beek, E. Pieterman, L. Cohen, C. Löwik, S. Papapoulos, *Biochem. Biophys. Res. Commun.* **1999**, *264*, 108–111; c) J. E. Dunford, K. Thomson, F. P. Coxon, S. P. Luckman, F. M. Hahn, C. D. Poulter, F. H. Ebetino, M. J. Rogers, *J. Pharmacol. Exp. Ther.* **2001**, *296*, 235–242; d) J. D. Bergstrom, , R. G. Bostedor, P. J. Masarachia, A. A. Reszka, G. Rodan, *Arch. Biochem. Biophys.* **2000**, *373*, 231–241.

[3] M. J. Rogers, D. G. Watts, R. G. G. Russell, *Cancer* **1997**, *80*, 1652–1669.

[4] a) A. Montalvetti, B. N. Bailey, M. B. Martin, G. W. Severin, E. Oldfield, R. Docampo, *J. Biol. Chem.* **2001**, *276*, 33 930–33 937; b) M. B. Martin, J. S. Grimley, J. C. Lewis, H. T. Heath III, B. N. Bailey, H. Kendrick, V. Yardley, A. Caldera, R. Lira, J. A. Urbina, S. N. J. Moreno, R. Docampo, S. L. Croft, E. Oldfield, *J. Med. Chem.* **2001**, *44*, 909–916; c) M. B. Martin, J. M. Sanders, H. Kendrick, K. de Luca-Fradley, J. C. Lewis, J. S. Grimley, E. M. Van Brussel, J. R. Olsen, G. A. Meints, A. Burzyńska, P. Kafarski, S. L. Croft, E. Oldfield, *J. Med. Chem.* **2002**, *45*, 2904–2914; d) Ch. M. Szabo, Y. Matsumura, S. Fukura, M. B. Martin, J. M. Sanders, S. Sengupta, J. A. Cieslak, T. C. Loftus, Ch. R. Lea, H.-J. Lee, A. Koohang, R. M. Coates, H. Sagami, E. Oldfield, *J. Med. Chem.* **2002**, *45*, 2185–2196; e) Ch. M. Szabo, M. B. Martin, E. Oldfield, *J. Med. Chem.* **2002**, *45*, 2894–2903.

[5] a) J. M. Sanders, A. O. Gómez, J. Mao, G. A. Meints, E. M. Van Brussel, A. Burzyńska, P. Kafarski, D. González-Pacanowska, E. Oldfield, *J. Med. Chem.* **2003**, *46*, 5171–5183; b) V. Yardley, A. A. Khan, M. B. Martin, T. R. Slifer, F. G. Araujo, S. N. J. Moreno, R.

Docampo, S. L. Croft, E. Oldfield, *Antimicrob. Agents Chemother.* **2002**, *46*, 929–931.
[6] a) T. H. Cromartie, K. J. Fischer, J. N. Grossman, *Pestic. Biochem. Physiol.* **1999**, *63*, 114–126; b) B. Lejczak, P. Kafarski, G. Forlani, H. Wojtasek, P. Wieczorek, *J. Plant Growth Regul.* **1996**, *15*, 109–113.
[7] P. Kafarski, B. Lejczak, G. Forlani, *Heteroat. Chem.* **2000**, *11*, 449–453.
[8] E. Kotsikorou, E. Oldfield, *J. Med. Chem.* **2003**, *46*, 2932–2944.
[9] E. Matczak-Jon, W. Sawka-Dobrowolska, P. Kafarski, V. Videnova-Adrabińska, *New J. Chem.* **2001**, *25*, 1447–1457.
[10] M. P. Jensen J. V. Beitz, R. D. Rogers, K. L. Nash, *J. Chem. Soc. Dalton Trans.* **2000**, 3058–3064.
[11] J. M. Sanders, S. Ghosh, J. M. W. Chan, G. Meints, H. Wang, M. Rake, Y. Song, A. Colantino, A. Burzyńska, P. Kafarski, C. T. Morita, E. Oldfield, *J. Med. Chem.* **2004**, *47*, 375–384.
[12] J. W. Steed, *CrystEngComm* **2003**, *5*, 169–179.
[13] A. R. Katritzky, C. W. Rees, *Comprehensive Heterocyclic Chemistry, Vol. 2*, Pergamon Press, Oxford (UK), **1984**, part 2A.
[14] E. Matczak-Jon, B. Kurzak, A. Kamecka, P. Kafarski, *Polyhedron* **2002**, *21*, 321–332.
[15] E. Matczak-Jon, B. Kurzak, A. Kamecka, W. Sawka-Dobrowolska, P. Kafarski, *J. Chem. Soc. Dalton Trans.* **1999**, 3627–3637.
[16] a) J. B. Lambert, S. I. Featherman, *Chem. Rev.* **1975**, *75*, 611–626; b) J. B. Lambert, D. S. Bailey, B. F. Michel, *J. Am. Chem. Soc.* **1972**, *94*, 3812–3815; c) F. A. L. Anet, I. Yavari, *J. Am. Chem.* Soc. **1977**, *99*, 2794–2796; d) A. M. Belostotskii, P. Aped, A. Hassner, *J. Mol. Struct. (THEOCHEM)* **1998**, *429*, 265–273; e) A. M. Belostotskii, H. E. Gottlieb, P. Aped, A. Hassner, *Chem. Eur. J.* **1999**, *5*, 449–455; f) A. M. Belostotskii, H. E. Gottlieb, P. Aped, *Chem. Eur. J.* **2002**, *8*, 3016–3026.
[17] a) F. A. L. Anet, I. Yavari, I. J. Ferguson, A. R. Katritzky, M. Moreno-Manas, M. J. T. Robinson, *J. Chem. Soc. Chem. Commun.* **1976**, 399–400; b) J. E. Anderson, A. I. Ijeh, Ch. Storch, D. Casarini, L. Lunazzi, *J. Org. Chem.* **1998**, *63*, 3310–3317.
[18] a) F. Suzuki, Y. Fujikawa, S. Yamamoto, H. Mizutani, C. Funabashi, T. Ohya, T. Ikai, T. Oguchi, *Ger. Offen* **1979**, 2831578; b) L. Maier, *Phosphorus Sulfur Relat. Elem.* **1981**, *11*, 311–322; c) J. Sołoducho, R. Gancarz, P. Wieczorek, J. Korf, J. Hafner, B. Lejczak, P. Kafarski, Patent PL 172268 B1, **1997**.
[19] Kuma Diffraction KM4CCD™ System Software, version 1.161, Kuma Diffraction Instruments GmbH, Wrocław (Poland), **1995–1999**.
[20] G. M. Sheldrick, SHELXS97, Program for the Solution of Crystal Structures, University of Göttingen (Germany), **1997**.
[21] G. M. Sheldrick, SHELXL97, Program for the Refinement of Crystal Structures, University of Göttingen (Germany), **1997**.
[22] SHELXTL version 5.10, Bruker AXS, Inc., Madison, Wisconsin (USA), **1997**.
[23] A. L. Speck, *J. Appl. Crystallogr.* **2003**, *36*, 7–13.

Received: April 7, 2004
Revised: September 9, 2004
Published online: January 24, 2005